

COMPOSITES, PART B, VOL. 33, 2002, 355-366**THE MECHANICAL PERFORMANCE OF REPAIRED STIFFENED PANELS:
PART II - FINITE ELEMENT MODELLING**

by

S MAHDI¹, A J KINLOCH², M A CRISFIELD³ & F L MATTHEWS⁴
IMPERIAL COLLEGE, LONDON, UK¹ *Mechanical Engineering Department & Centre for Composite Materials;
currently at CCM, University of Delaware, USA*² *Mechanical Engineering Department*³ *Aeronautics Department*⁴ *Centre for Composite Materials***ABSTRACT**

In this paper the finite element modelling under compressive static load of I-section stiffened panels is reported. A pristine panel is compared with panels containing simulated damage and repaired panels. Predicted stiffness, stress distributions and strength of the panels are compared with experimental results.

1. INTRODUCTION

In Part I of this paper [1] the experimental characterisation of pristine, 'damaged' and repaired stiffened panels was presented. Strength, stiffness, strain distributions and failure modes were described, and it was shown that the repaired panels recovered a high fraction of the strength of the pristine, undamaged, panel. As noted before, the work described in [1] was part of a much wider investigation in which the repair of sandwich beams was also studied [2].

In the current paper the finite element (FE) modelling of the panels is described. The objective of this modelling work was to develop a simple FE method that could be used for the design of repairs to I-stiffened panels. The FE method was used to calculate the stiffness and strain distribution for the panels. The FE results were then compared with the experimental data. Additionally, an attempt to calculate the strength of the panels with a widely used (and a widely implemented) failure criterion is discussed.

2. THE FINITE ELEMENT MODELS**2.1 Introduction**

The quasi-three-dimensional approach, which uses composite shell elements, was used to model the behaviour of the stiffened panels in compression. The LUSAS (FEA Ltd.) FE package was employed.

The undamaged panel (P1) was first modelled, and two different analyses were done. In one case the response of the material and the panel was assumed linear elastic, whereas in the other the panel's geometric response only was assumed non-linear elastic. One damaged and one repaired panel were subsequently modelled, using the same approaches. The panel damaged by the through-hole only (P2) was modelled in the present work. The equivalent repaired panel (P4) was also modelled (see [1] for details of panels).

The FE load-displacement and displacement-strain responses are compared with experimental results. The stress resultants in the panels are then subsequently used in conjunction with the Tsai-Hill failure criterion to estimate the failure load of the panels.

2.2 FE Model Definition

2.2.1 Introduction

The FE meshes were created using the LUSAS graphics pre-processor. The models included the skin and the three stiffeners, but no attempt was made to model the aluminium C-sections in which the ends of the panels were potted [1, 2]. The total length of the panels was however included in the geometry and the effect of the C-section on the loaded edges of the panels was modelled by preventing appropriate displacements or rotations, as will be shown later.

The skin and the stiffeners were modelled using quadrilateral, linear, thick shell elements (QTS4). The QTS4 elements are capable of modelling composite properties as well as geometric non-linearity. For these elements five degrees of freedom (three translations and two in-plane rotations) are usually associated with each node. However, these elements may be used for modelling intersecting shells (i.e. stiffened shell structures) where the shells may be connected to three-dimensional (3D) beam elements, and in this instance six degrees of freedom are automatically defined. Some simplifications have, however, to be taken into account in order to model the skin-stiffener attachment. Figure 1 shows a cross-section of the skin-stiffener junction, as well as its FE idealisation.

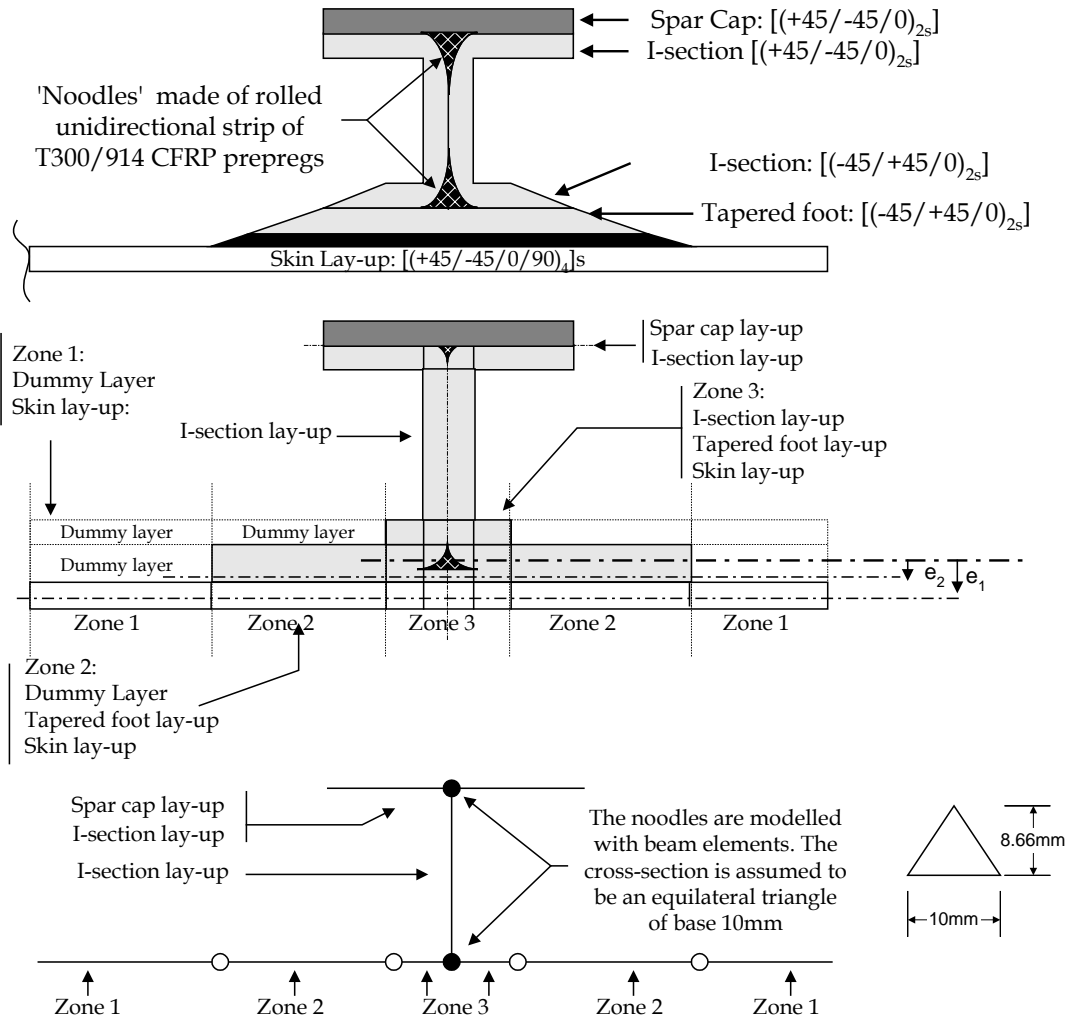


Figure 1: Cross-sectional view of the skin-stiffener attachment and its equivalent shell element modelling approach

The cross-section of the skin/stiffener junction was separated into three zones. The first zone consisted of the skin of the panel, the second consisted of the skin and the tapered foot of the stiffener, and the third zone consisted of the skin, the tapered foot and the base of the stiffener's I-section. Because of the different thicknesses and lay-ups of the sections, an appropriate number of 'dummy' layers was added in zone 1 and zone 2 to make up the maximum number of layers; the numbers of layers then being the same across the entire model. The material in the 'dummy' layers had very low stiffness properties, so that they would not influence the behaviour of the structure.

It was shown in [1] that significant bending of the skin may occur under load. However, since in a shell element the nodal plane may not correspond with the bending plane for the structural element being modelled, an eccentricity must be defined. In the present work the centroid of the section defined in zone 3 was taken as the reference plane for

bending of the structure; an eccentricity e_1 and e_2 was defined for the sections in zone 1 and 2, respectively (i.e. $e_1=0.915\text{mm}$ and $e_2=1.83\text{mm}$), as shown in Figure 1.

The two triangular sections in the stiffeners that are seen in Figure 1, made of strips of rolled unidirectional CFRP prepregs, called ‘noodles’, were also modelled. The noodles were modelled as triangular sections using 3D beam elements (BTS3). It is noted that the BTS3 elements do not support composite properties, and they were therefore modelled as isotropic solids. The beams were placed so that they connect the stiffeners to the skin, and the top of the stiffeners to the web of the stiffeners as shown in Figure 1.

The skin and noodles are made from T300/914 fabric with the mechanical properties shown in Table 1 [3]. The moduli in the table were obtained from tension tests. However, the loading on the panels is compressive, so a reduced compressive modulus of $E_1=119\text{GPa}$ was used, as is common for CFRP components [4].

Table 1: Properties of the materials used on the stiffened panels

	T300/914C	Redux 319 Adhesive
E_1 (GPa)	139	3.78
E_2 (GPa)	9.5	3.78
E_3 (GPa)	9.5	3.78
ν_{12}	0.32	0.4*
ν_{21}	0.02	0.4*
ν_{23}	0.5	0.4*
ν_{13}	0.32	0.4*
G_{12} (GPa)	5.4	1.35
G_{13} (GPa)	5.4	1.35
G_{23} (GPa)	3.6	1.35
S_1 (Tension) (MPa)	1490	64.5
S_1 (Compression) (MPa)	1402	-
S_2 (Tension) (MPa)	46	64.5
S_2 (Compression) (MPa)	215	-
S_3 (Tension) (MPa)	46	64.5
S_3 (Compression) (MPa)	215	-
S_{12} (MPa)	79	60

* *estimated properties*

The boundary conditions on the potted ends were idealised so as to prevent all displacements and rotations. An applied (vertical) displacement was imposed at one end of the panel, whereas the other end was fully constrained.

A linear elastic and geometrically non-linear elastic analysis were performed. The geometric non-linear analysis was performed using a total Lagrangian formulation. For each load increment a standard Newton-Raphson iterative procedure was used, as this has been shown to be effective for this type analysis [5].

2.2.2 Undamaged panel

The mesh used for the undamaged panel contained twenty four elements along the length and twenty four elements across the width. The stiffeners were modelled with two elements along the depth of the web and two elements across the width of the spar cap. An area across the ends of the panel, corresponding to the potted region, was subjected to the boundary conditions.

2.2.3 Damaged panel

The mesh used for the panel damaged with a through-hole (P2) was identical in principle to that for the undamaged panel and is shown in Figure 2. The geometry and the mesh spacing has been altered appropriately to take into account the cut-out. The majority of elements for the skin and the stiffeners were quadrilateral elements (QTS4), with a few three-node triangular elements around the hole.

2.2.4 Repaired panel

For the panel with a repaired through-hole (P4), the patch was simplified in the FE model in order to avoid using an excessive number of elements. The modelling approach used is identical in principle to the one described above. As the two side stiffeners were unaffected by the damage and the repair, they were therefore modelled as was shown in Figure 2.

However, the lay-up of the panel around the central stiffener had to take into account the repair patches. The panel was again separated into zones as shown in Figure 3. Because of the different thicknesses and lay-ups of the sections, an appropriate number of 'dummy' layers was added in the different zones to make up the maximum number of layers. The offset in the local neutral axis introduced by the patch was modelled. The material that comprises the patch was assumed to have properties identical to the parent materials, as defined in Table 1.

In Figure 3, the area affected by the repair patch (on the stiffener side) is shown highlighted. The mesh for the repaired panel was identical to the mesh for the undamaged panel.

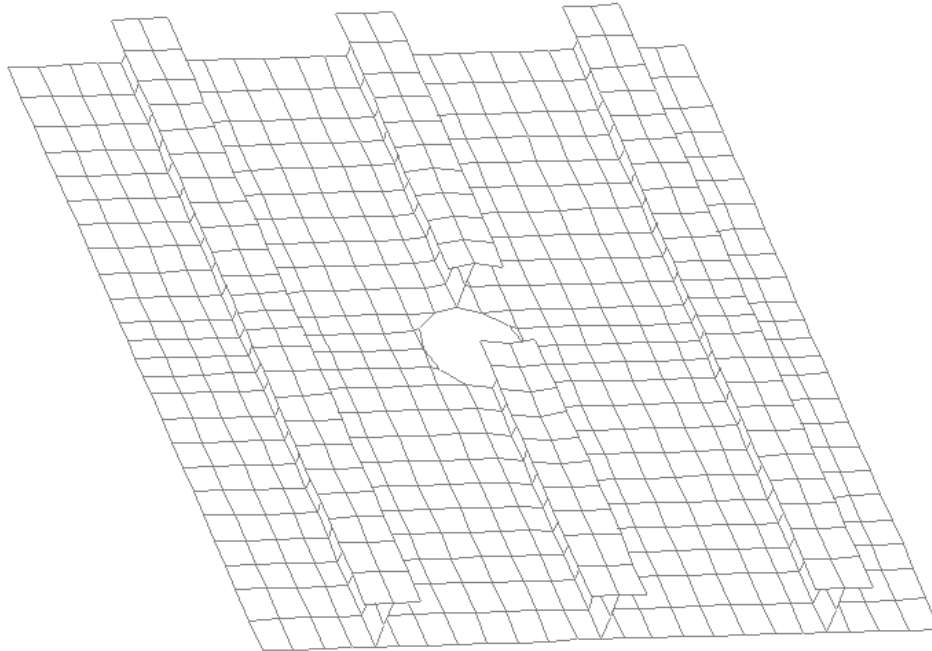
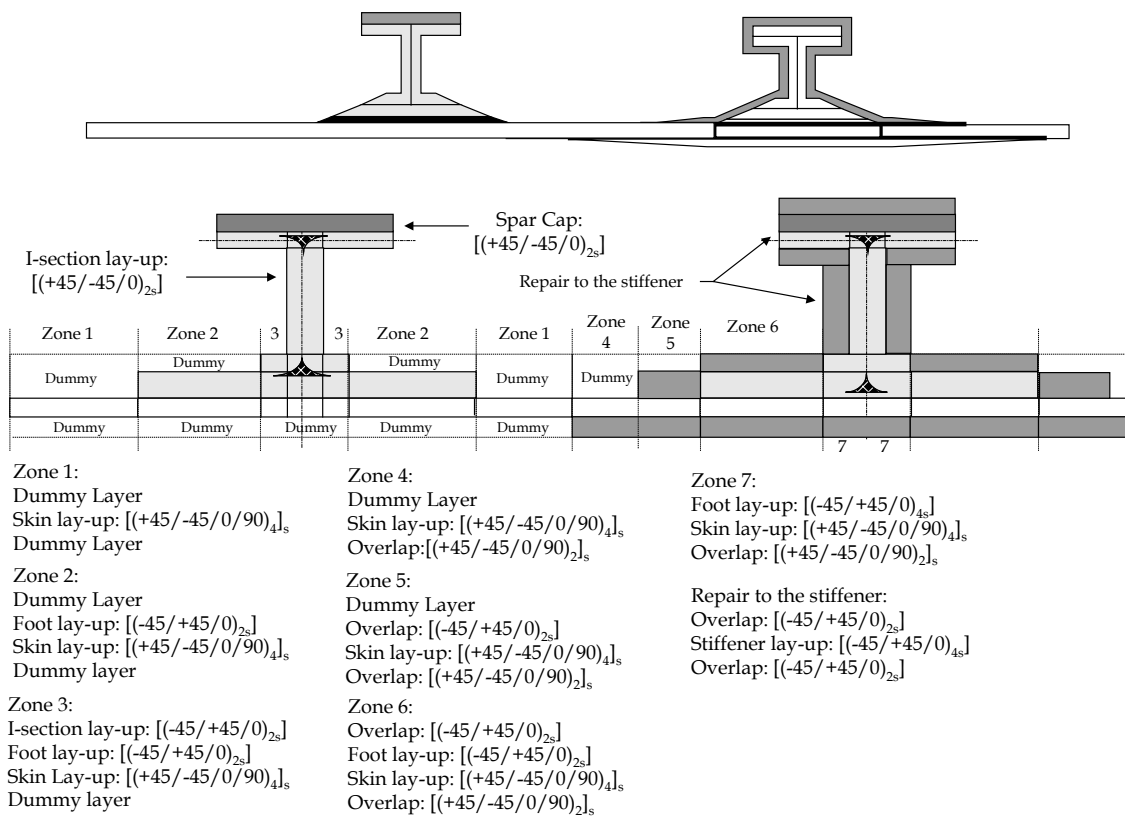


Figure 2: Finite element mesh of the damaged panel (P2)



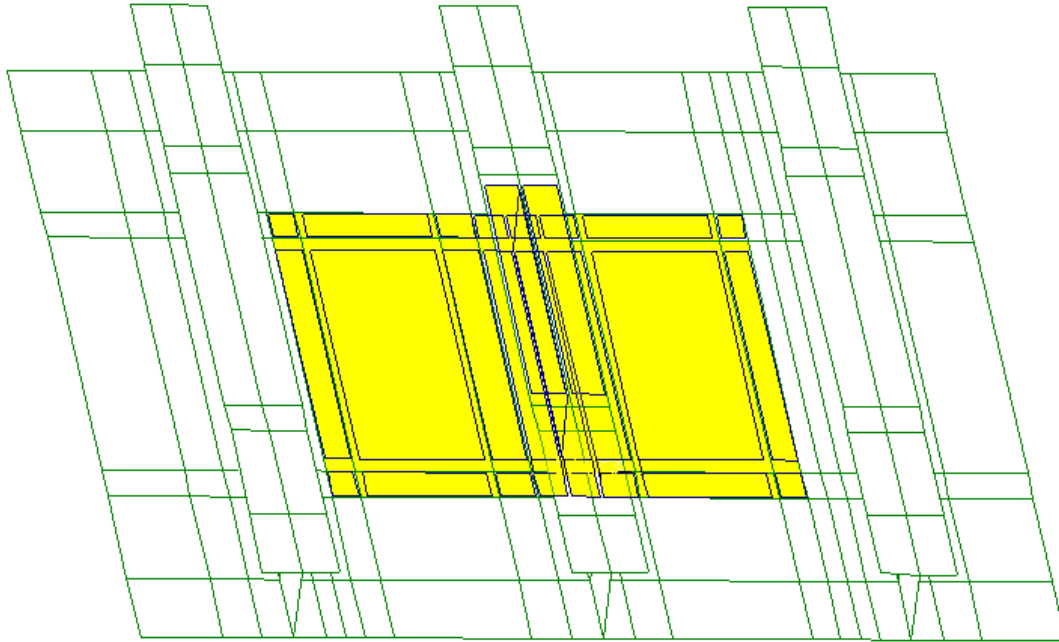


Figure 3: Cross-sectional view of the skin-stringer attachment on the repaired panel and its equivalent shell elements modelling approach
(the area covering the overlap repair patch is highlighted)

3 STIFFNESS PREDICTIONS

3.1 Undamaged panel (P1)

The meshes of the deformed undamaged panel for the linear elastic and the geometrically non-linear elastic analyses are shown in Figure 4. The deformed meshes were magnified at an applied displacement shown in brackets for each of the panels. It may be seen in Figure 4 that the linear elastic analysis predicts that the initially flat undamaged panel deforms in a complex manner and, whereas the central part of the panel remains fairly flat, deformation occurs at the unsupported edges due to the complex load path in the panel. On the other hand it may be seen that the non-linear analysis of the undamaged panel resulted in a different deformed mesh than for the linear analysis. The unsupported edges and the skin bays (i.e. the skin between the stiffeners) deformed in a two-dimensional wavy pattern. A total of four half-wavelengths developed in the panel. The unsupported edges and the skin bay are predicted to buckle between the stiffeners, which have remained essentially undistorted.

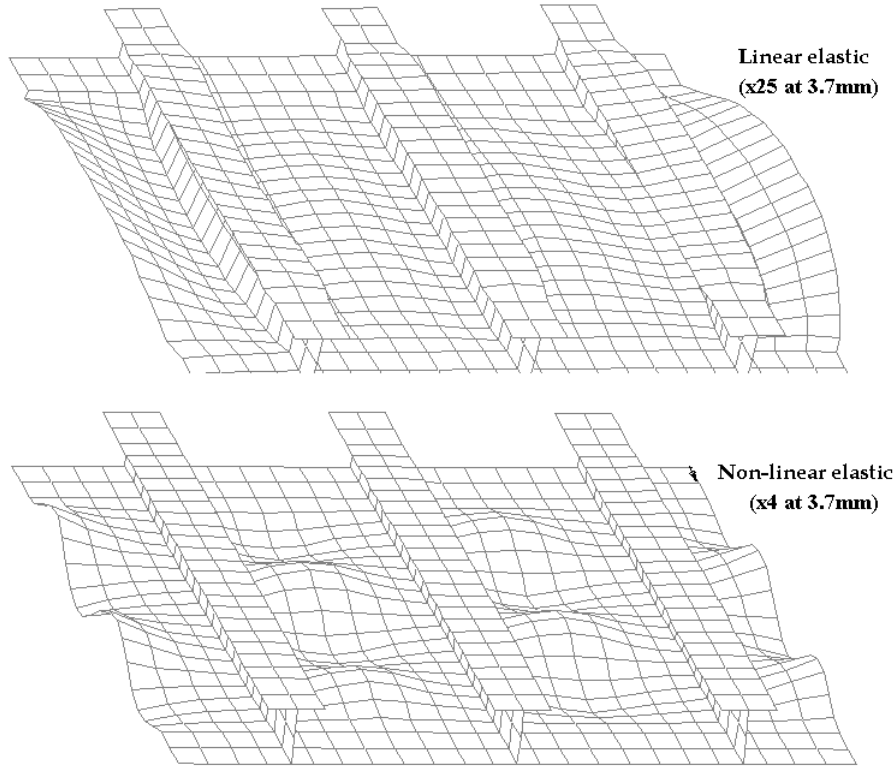


Figure 4: Finite element meshes of deformed undamaged panel (P1)

The load-displacement curves obtained from the linear and non-linear elastic FE analyses are compared in Figure 5 with experiment data [1]. The non-linear results show good correspondence with the experimental load-displacement curve. Only when the applied displacement approaches the failure displacement do the curves diverge slightly, and this may be due to progressive damage developing in the panel that was not modelled in the present analysis. On the other hand, it may be seen that the linear elastic analysis yields a stiffer prediction. The experimental and linear elastic curves correspond for small applied displacement, i.e. below 0.5mm, after which they separate. The correspondence of all the curves at low applied displacement was to be expected since non-linear geometry and damage evolution are only likely to have an effect at higher applied displacements.

The experimentally measured back-to-back far field strains at the edge of the panel (SG1 and SG2) [1], are compared with strains obtained from the FE analyses in Figure 6. The strains on the skin and stiffener sides are shown for comparison. The averaged FE strains were for an element located 130mm from a loaded end, and 15mm from an unsupported edge (i.e. the location of the SG1 and SG2 strain gauges).

Although the experimental and computed strains were comparable at low applied displacement, the predictions diverged above 2.6mm applied displacement with the SG1 values being better predicted by the non-linear analysis, and the SG2 values by the linear analysis. The non-linear elastic analysis indicates that the panel buckled at about 2.6mm

applied displacement. Such a pronounced deviation in the strains was however not observed experimentally.

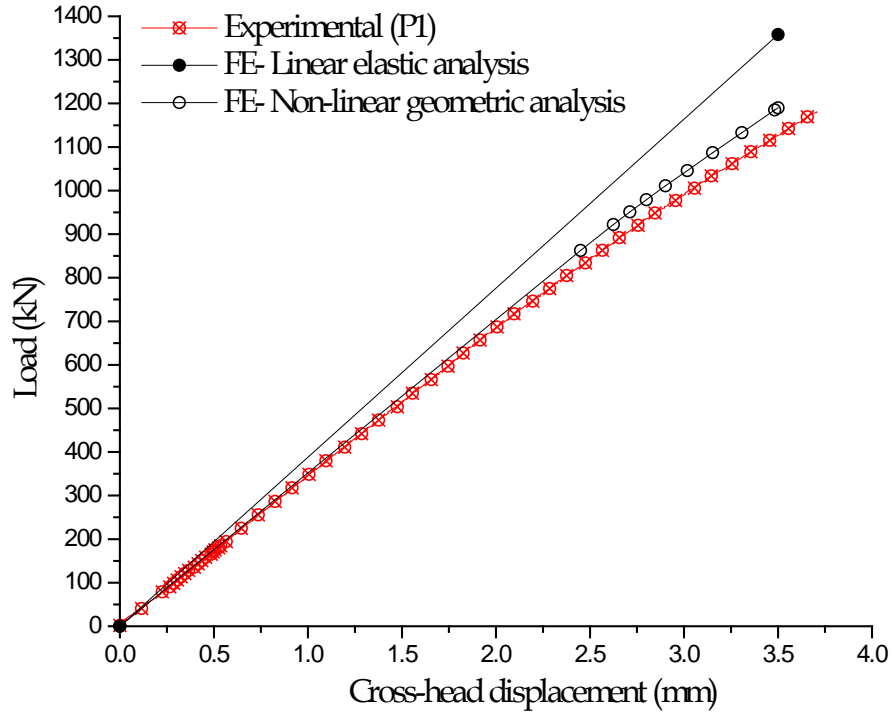


Figure 5: Experimental and computed load-displacement curves (panel P1)

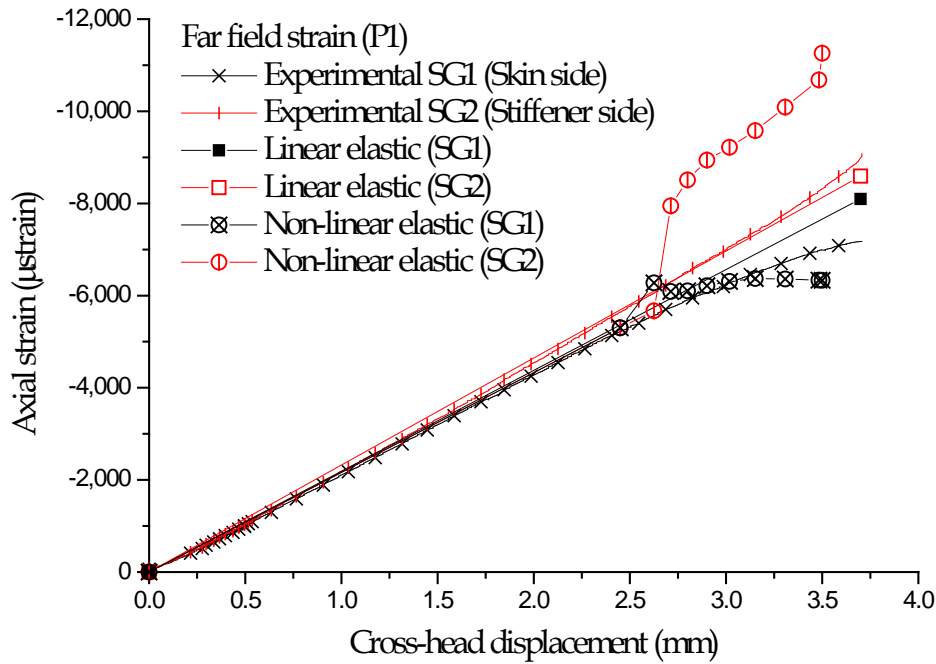


Figure 6: Experimental and computed strain-displacement curves (panel P1)

The axial strains were found to vary periodically along the length of the panel, and in sympathy with the buckle mode shape seen in Figure 4, the strain being maximum at the buckle peaks. The strains on the stiffener and the skin side are asymmetric, and can be compressive or tensile, as a result of the local curvature induced by the buckled mode shape. As a result, the strains on the stiffener and the skin faces will either be increased or decreased relative to the average applied strain.

Since the strain gauges measure strains averaged along their 6mm length, there will be a limit to the ability of strain gauges to accurately record the strain field. Indeed, if the gradient in strains along the buckled edge is large, this will lead to differences when comparing calculated FE strain outputs with experimental strains, as was shown in Figure 6. The location of the strain gauge will also be of importance.

3.2 Damaged panel (P2)

The deformed meshes from the linear elastic and non-linear elastic analyses of the damaged panel are shown in Figure 7. First, it may be seen that the deformed meshes, whether from a linear or a non-linear elastic analysis, are essentially the same. As might be expected, the damaged panel is predicted not to deform in the same way as the undamaged panel did. Having been cut, the central stiffener is of a limited use in supporting the bay skin and the central part of the panel is seen to have deformed out of the plane. This behaviour will account for the marked decrease in stiffness and in failure load recorded in the experiment [1]. The load path for this panel is directed around the

cut-out and towards the side stiffeners, which are nevertheless predicted to remain flat and not significantly distort.

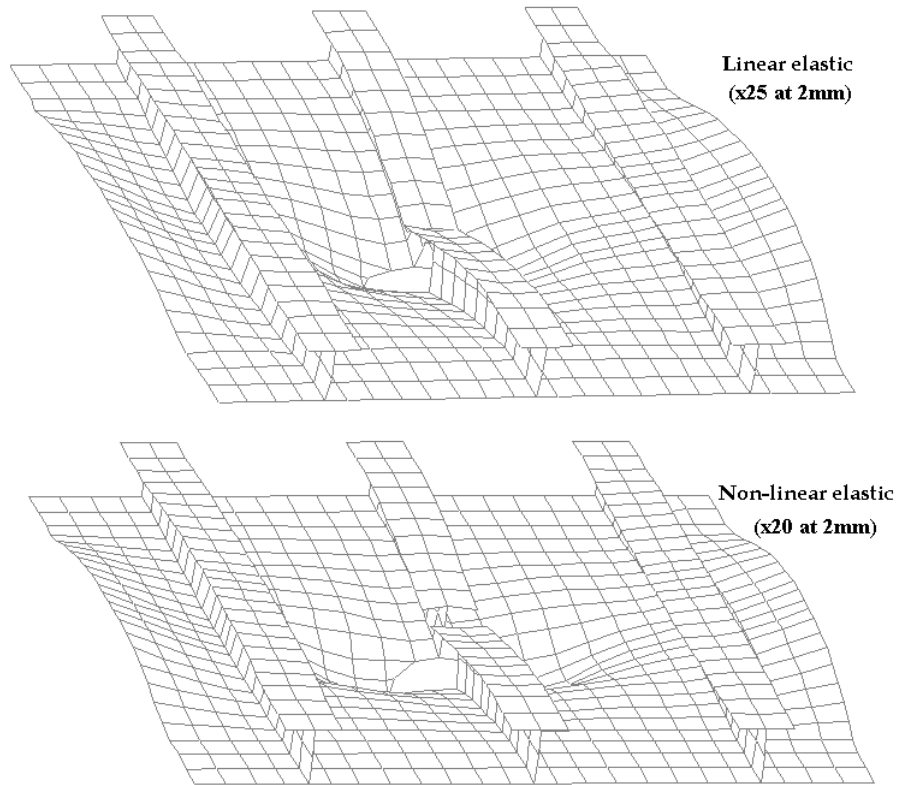


Figure 7: Finite Element meshes of deformed damaged panel (P2)

The linear elastic and the non-linear elastic load-displacement predictions are compared with experiment in Figure 8. An excellent agreement is seen between the non-linear elastic FE and the experimental responses. The agreement is still very good between the linear elastic FE and experimental responses, although the curves diverge when approaching the failure displacement. It is recalled that, in Figure 7 the deformed meshes of the damaged panel showed only minimal deformation at the unsupported edges; the panel was not predicted to buckle and this may explain the good agreement between the FE and experimental results.

It was found [1] that the experimental strains recorded at 15mm from the cut-out (SG18) were 2.4 times the far field strain (SG2). For clarity, only the experimental and FE strains on the stiffener side are compared in Figure 9.

It may be seen in Figure 9 that both the linear and non-linear FE and the experimental far field strains (SG2) are in very good agreement. However, the choice of analysis (i.e. linear or geometric non-linear) has had an influence on the prediction of strains near the cut-out. The experimental (SG18) and linear FE strains seem to agree for low applied

displacements, although the curves diverge significantly above 0.5mm displacement. The damaged panel was seen in Figure 7 to deform significantly at its centre, which resulted in the increase in strain around the damage. It may be that the linear analysis is inadequate in this case because of the large deformation occurring at the centre of the panel. Indeed, the non-linear FE analysis may be seen, in this case, to lead to the better predictions, although the strains at failure are over-predicted significantly (see below).

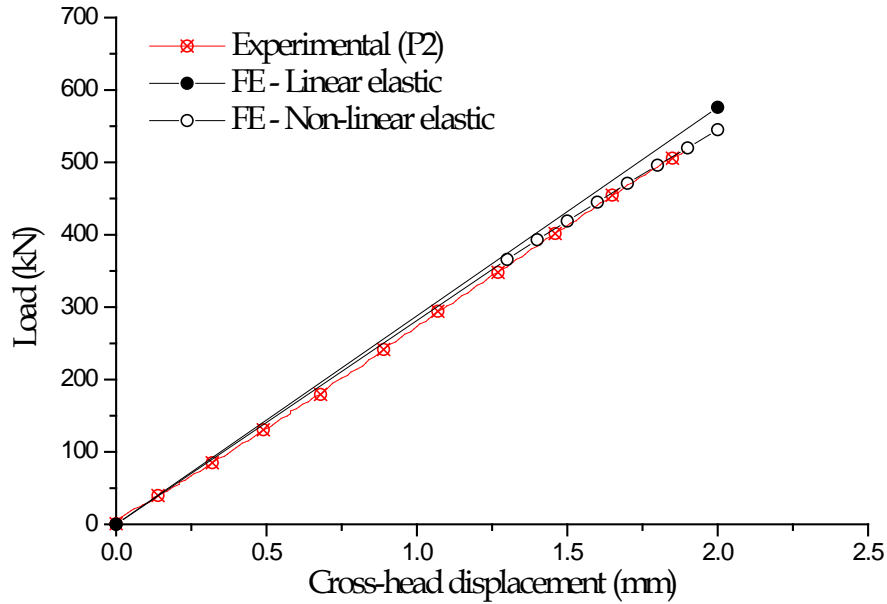


Figure 8: Experimental and computed load-displacement curves (panel P2)

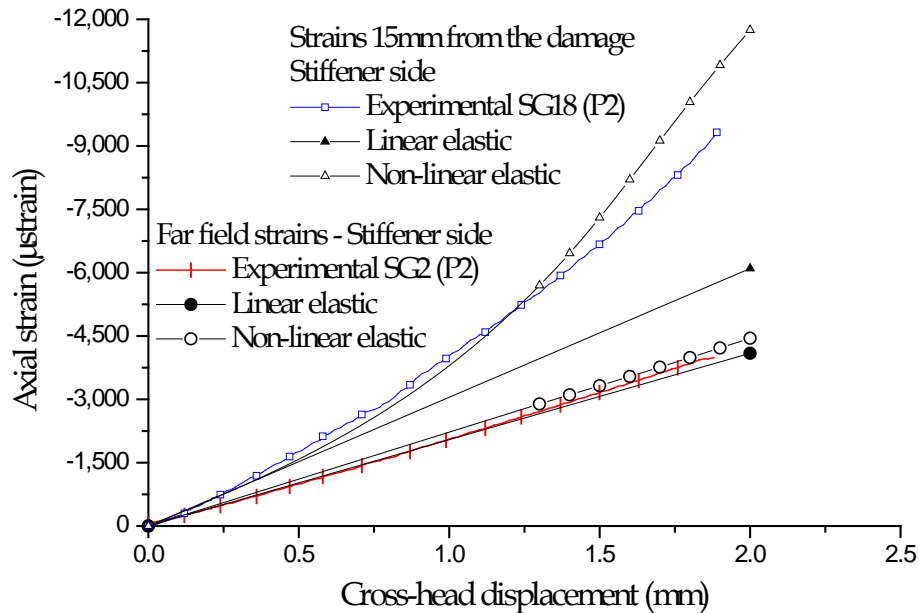


Figure 9: Experimental and computed strain-displacement curves (panel P2)

3.3 Repaired panel (P4)

The deformed meshes for the repaired panel may be seen in Figure 10. The deformation is more complex than for the undamaged and damaged panels. The portion of the panel covered by the overlap repair patches (i.e. the region highlighted by the darker mesh) remains fairly flat. The extra thickness provided by the patches stabilises the centre of the panel. The portions of skin bay between the potted ends and the repair patch deforms significantly out of the panel's plane; four 'pockets' may be seen to have formed at these regions. However, these 'pockets' do not result from buckling deformation, but rather from the transition between the thick, patched area, to the unsupported thin skin area. The only noticeable difference between the deformed meshes from the linear and non-linear analyses may be seen at the unsupported edges of the panel. The unsupported edges are predicted to remain flat or to buckle according to whether a linear or a non-linear elastic analysis is done; a conclusion similar than for the undamaged panel. It is noted, however, that only three half-wavelengths are now predicted, rather than four for the undamaged panel.

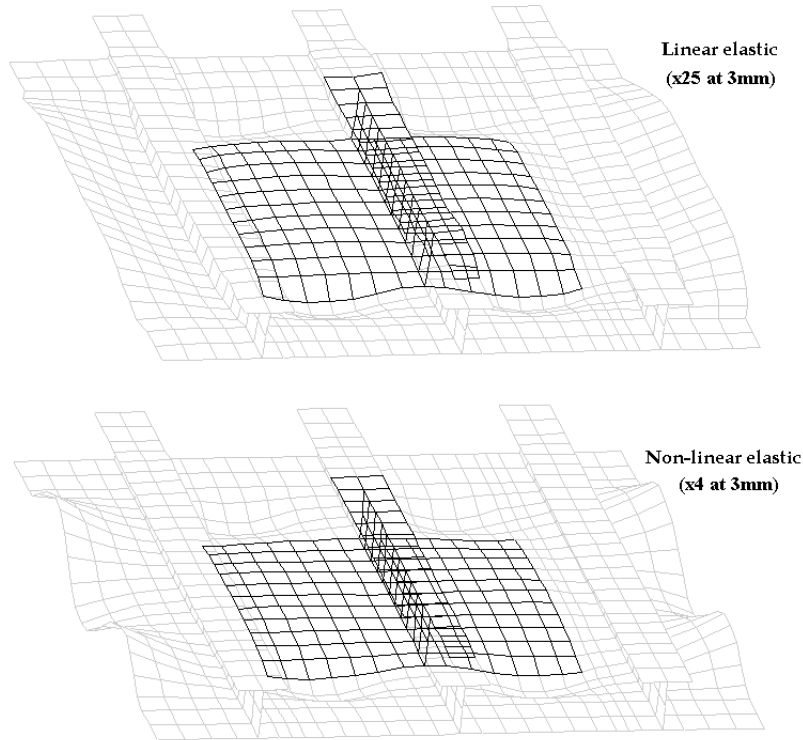


Figure 10: Finite Element meshes of deformed repaired panels

When the linear elastic and the non-linear elastic FE responses for the repaired panel are compared with experiment, the load-displacement slopes of the FE results show very good agreement with experiment. However, the experimental load-displacement curve has an s-shape, and as a result crosses the calculated FE responses for applied displacement between 0.5 and 1mm. The agreement with experiment is nevertheless very good if the slopes of the curves are compared, as shown in Figure 11.

The strains in the repair patch (e.g. SG18) are lower than the far field strains (e.g. SG2) [1] since the excess material provided by the patch protects the damaged area and results in a decrease in strain in the vicinity of the cut-out. The predicted far field strain from the linear elastic analysis was in good agreement with experiment. The prediction from the non-linear elastic analysis, however, was not quite so good, as seen in Figure 12.

Also, the predicted strains in the repair were calculated to be lower than the measured strains. This may be as a result of the modelling approach. In [1] it was shown that the repair patch was graded in size to avoid excessive development of peel stresses at the overlap edge. The patch was, however, idealised in the FE model with a constant thickness and as a result leads to a stiffer prediction than experiment. It is noted that a finer idealisation of the repair patch is possible, although with an associated extra degree of complexity in the model.

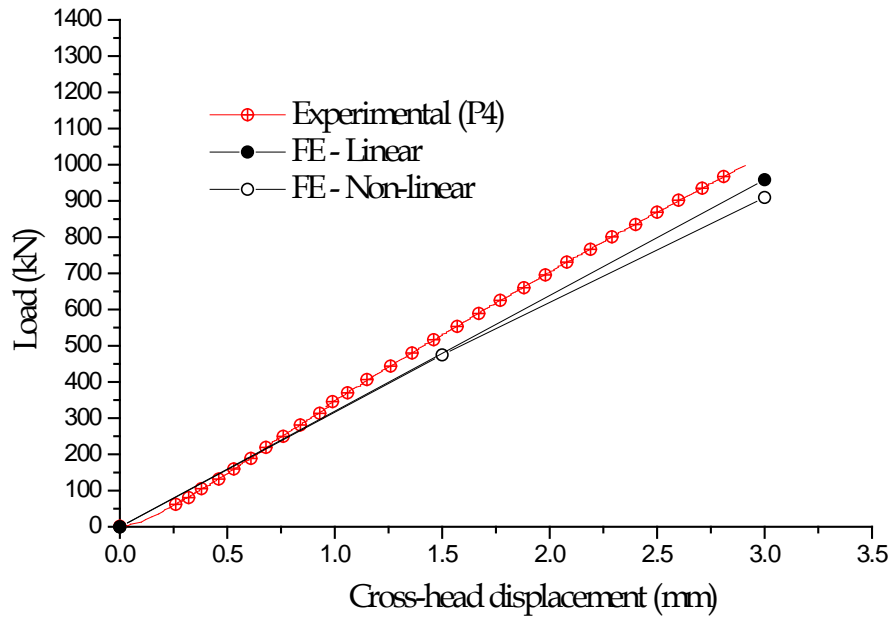


Figure 11: Experimental and computed load-displacement curves (panel P4)

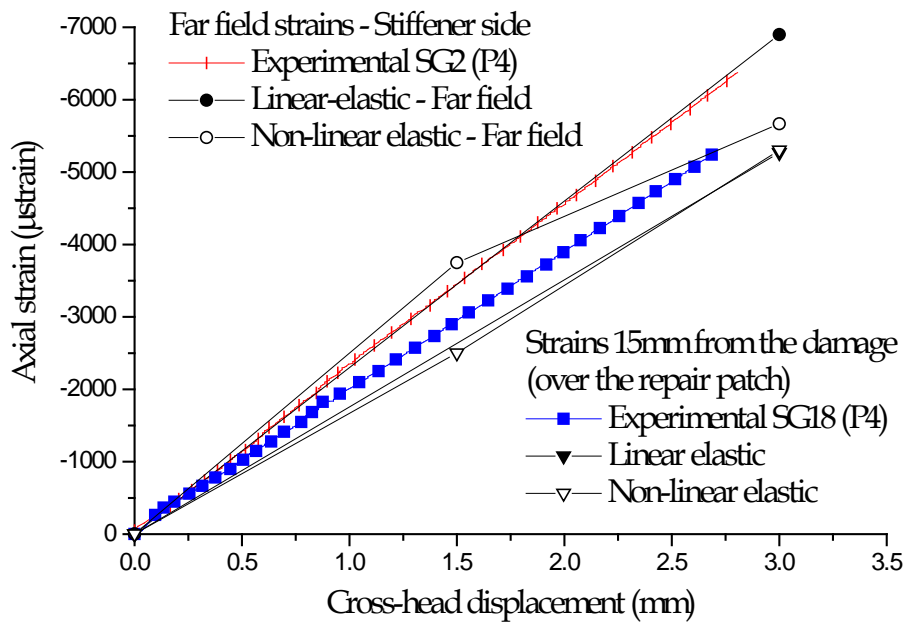


Figure 12: Experimental and computed strain-displacement curves (panel P4)

4. PREDICTION OF FAILURE

4.1 Introduction

There exist a number of locations in the panels where failure could have initiated. For instance, failure could have resulted from the separation of the stiffeners from the skin as documented in references [6, 7, 8], or by an interlaminar shear failure of the stiffener web, as was found by Falzon et al. [9]. However the aforementioned literature refers to panels having a failure load several times (e.g. two to three times) the initial buckling load. The type of panel investigated in the present study, being relatively thick, does not deform as much as a panel that is expected to work in the post-buckled region. Although buckling was predicted here for the undamaged panel, the deformation would have been relatively small since the shadow Moiré technique did not detect any such deformation. Furthermore, in the present work the percentage difference in back-to-back strain at the edge of the undamaged panel was calculated to be 23% at failure, whereas it was calculated to be as much as 800% in reference [9]. The present panels are not therefore thought to buckle to any great extent, and in-plane material failure, such as the failure of the skin or of the stiffeners, may be thought to precede the separation of the stiffeners from the panel.

It is proposed in this section to estimate the failure displacement of the undamaged, damaged and repaired panels from the FE results. There are a number of failure criteria that exist to predict the failure of composite structures [2]. Amongst them is the Tsai-Hill criterion that produces a smooth failure envelope from which the failure loads may be estimated. However, there are many distinctly different modes of failure for fibre-composites structures. These include fibre failure, buckling and matrix failure, etc. Thus, it is generally recognised that it is inappropriate to have a smooth failure envelope that can effectively represent many distinct failure mechanisms. However, progressive damage analyses are not widely available for FE codes and the hence the Tsai-Hill criterion was used.

To undertake this aspect of the modelling, the shell elements used in these FE models can identify layer orientations and they can therefore be employed to calculate results such as strain and stress fields for each layer that composes the shell. However, the runs were carried out on a PC with a limited amount of memory and it was not possible to output the results for each layer. It was nevertheless possible to read the stress resultants for each node, and these were used, in conjunction with laminate analysis software, to calculate the equivalent stresses in the panels. The calculated stresses were then used in conjunction with the Tsai-Hill criterion (Equation 1), and appropriate scaling, to predict the failure displacement.

$$\frac{\sigma_1^2}{S_1^2} - \frac{\sigma_1\sigma_2}{S_1^2} + \frac{\sigma_2^2}{S_2^2} + \frac{\sigma_{12}^2}{S_{12}^2} \geq 1 \text{ at failure} \quad (1)$$

4.2 Undamaged panel (P1)

Contour plots of stress and moment resultants were computed from the geometrically non-linear analysis at the experimental failure displacement.

It was seen that the in-plane load in the undamaged panel was uniformly carried by the stiffeners and the skin bays. The stiffener feet seemed to carry the highest load as a result of the increase in thickness provided by the stiffener foot over the skin. The unsupported edges carried little load. It was also noted that the in-plane stress resultant carried by the skin bays was a minimum at their centre as a result of local bending. It was found that the stiffeners carry virtually no bending moment in the axial direction; the stiffeners were not predicted to deform out of the plane.

It was suggested from the experimental studies [1] that the collapse of the undamaged panel could have resulted from an in-plane compressive failure of the skin. The latter seems to correlate with the calculated results, since the analysis predicts that the maximum in-plane stress and moment resultants are carried by the skin at a buckle crest.

The stress resultants, at an applied displacement of 3.7mm (i.e. the experimental displacement at failure), taken in the skin bay are shown in Table 2. Results from the linear elastic and non-linear elastic models are compared in the table. The stress resultants were read at the centre of a skin bay and at a buckle crest where the stresses are maximum due to the large bending deformation.

The laminate analysis software LAP [10] was then used to calculate the stresses in a laminate, having the lay-up of the panel's skin, and subjected to the stress resultants shown in Table 2. The stresses, calculated from LAP for each ply, were subsequently used in conjunction with the Tsai-Hill criterion (Equation 1) to assess proximity to failure.

When stresses and strengths (from Table 1) were used in Equation 1, the Tsai-Hill criterion predicted initial failure to be in the +45° outermost ply, for both types of analysis, as shown in Table 2. The predicted failure location accords well with the experimental observation. Furthermore, since the Tsai-Hill index (left-hand side of Equation 1) is close to unity, it can be said that the analysis, which was based on the experimental failure displacement, gives a prediction which is in good agreement with that observed experimentally, whether calculated from the linear elastic or the non-linear elastic FE analysis.

Table 2: Computed stress resultants for a node at mid-length and in the skin bay of the undamaged panel (P1); 3.7mm applied displacement

	N_x (N/mm)	N_y (N/mm)	N_{xy} (N/mm)	M_x (N)	M_y (N)	M_{xy} (N)	Tsai-Hill indices ⁺
Mid-bay (linear)	-1398	-74	9	-1162	-79	6.6	1.09
Mid-bay (non-linear)	-1036	48	22	-1364	-303	24	0.99

⁺ The Tsai-Hill indices are given for the outermost +45° ply

4.3 Damaged panel (P2)

Contour plots of stress and moment resultant in the loading direction for the damaged panel were computed from the geometrically non-linear analysis for the experimental failure displacement.

It was seen that the presence of the cut-out significantly changed the load path in the panel. The central stiffener was ineffective in carrying the axial load, which was carried by the side stiffeners and the skin around the damage. The in-plane stress resultant was maximum at the edge of the damage (cut-out).

Furthermore, it was seen that the moment resultant carried by the damaged panel had its maximum and minimum at the edge of the cut-out. A positive maximum value was seen at the edge of the cut-out and at the mid-length of the panel. Similarly, a negative maximum (i.e. minimum) value was also seen at the edge of the cut-out, but at approximately 45° from the loading direction. It is the presence of the cut-out that results in an increase in moment resultant carried by the side stiffeners, whereas they were shown not to carry any moment in the undamaged panel.

To estimate the failure displacement only results from the geometrically non-linear FE analysis were used, since the agreement between the experimental values and the predicted linear FE axial strains near the cut-out was poor (see Figure 9). The stress resultants at the edge of the cut-out for an applied displacement of 1.88mm (i.e. the experimental displacement at failure) are shown in Table 3.

The stresses in each ply of a laminate having the skin's lay-up, and subjected to the stress resultants shown in Table 3, were calculated using LAP [10]. The calculated stresses were then used with the Tsai-Hill criterion (Equation 1) to predict failure. Failure of the outermost 0° ply was predicted to occur first, although at a much lower displacement than that seen in the experiment. The corresponding Tsai-Hill index is 1.93 and, assuming a linear elastic relationship in the load-displacement response (which agrees with experiment [1]), the predicted failure displacement is 1.35mm (i.e., $1.88\text{mm}/\sqrt{1.93}$). Thus, the predicted failure displacement is about 28% lower than experiment.

One possible reason for the difference may be the coarse mesh used to model the cut-out, and a better agreement between FE and experiment might have been found if mesh refining had been done, or if higher-order elements had been used around the cut-out. This issue was not investigated in the present work. Also, progressive damage of the area will take place around the cut-out at relatively high applied displacements, and this was not modelled by the present analysis.

Table 3: Computed stress resultants for a node at the edge of the cut-out of the damaged panel (P2); 1.88mm applied displacement

	N_x (N/mm)	N_y (N/mm)	N_{xy} (N/mm)	M_x (N)	M_y (N)	M_{xy} (N)	Tsai-Hill index ⁺
Mid-bay (non-linear)	-3158	-329	20	801	394	25	1.93

+ The Tsai-Hill index is given for the outermost +0° ply

4.4 Repaired panel (P4)

Finally, contour plots of stress and moment resultant in the loading direction for the repaired panel were computed from the geometrically non-linear analysis at the experimental failure displacement.

The load path in the panel was seen to have been restored, although the present repair scheme has slightly over-stiffened the skin bays, as a result of the increase in thickness provided by the repair patches. The central stiffener was also found to support more load than the side stiffeners and this may be seen as a result of the patch interacting with the stiffener.

It was found that the presence of the repairs prevented the stiffeners from carrying any moment resultant, as for the undamaged panel. The repair patch stabilised the central stiffener as well as the skin around the cut-out. However, the moment resultant at the edges of the overlap patch was high when compared with that of the rest of the repair patch. This is a result of the geometric transition between the thick patch to the unsupported (thin) skin of the panel.

The method used to estimate the failure displacement of the damaged panel was used to estimate the failure displacement of the repaired panel. The failure of the panel was assumed to have resulted from in-plane material failure in the skin bay (now comprising the overlap patch on the skin and the stiffener sides). Again, results from the geometrically non-linear analysis only were used.

The calculated stress resultants at an applied displacement of 2.91mm (i.e. the experimental displacement at failure) are shown in Table 4. As before, the LAP [10] software was used to calculate the stresses in a laminate with a lay-up that comprised the skin and the overlap repair patches, and was subjected to the values of stress resultants shown in Table 4. The calculated stresses were then used with the Tsai-Hill criterion to

calculate the failure index. Failure of the outermost 0° ply (i.e. in the overlap patch on the stiffener side) was predicted to occur first.

Table 4: Computed stress resultants for a node at the edge of the cut-out of the repaired panel (P4); 2.91mm applied displacement

	N_x (N/mm)	N_y (N/mm)	N_{xy} (N/mm)	M_x (N)	M_y (N)	M_{xy} (N)	Tsai-Hill index +
Mid-bay (non-linear)	-1470	-249	191	-2400	-582	268	0.387

+: The Tsai-Hill index is given for the outermost $+0^\circ$ ply; hence in the repair overlap

Assuming a linear elastic relationship in the load-displacement response the predicted failure displacement is 4.68mm (i.e., $2.91/\sqrt{0.387}$). This value is 61% higher than the actual displacement of 2.91mm of the repaired panel, and higher even than the 3.7mm displacement for the undamaged panel

5 DISCUSSION

5.1 Undamaged panel

It has been shown that the load in the undamaged panel is carried by the stiffeners as well as by the skin bays. The unsupported edges were shown to support less load than the skin bays. The moment resultant in the direction of loading was furthermore seen to vary periodically in the skin bay, having maxima at the buckle crests. The skin bay was therefore shown to have a high in-plane stress resultant as well as a high moment resultant at buckle crests; thus it may be expected that the collapse of the undamaged panel will occur at one of the peaks. The stress resultant at a buckle peak was used to estimate failure and it was shown that the Tsai-Hill criterion predicts failure of the skin bay at the experimental failure displacement. The results from the linear elastic and the non-linear elastic analysis were used to estimate failure, and both methods were seen to show good agreement with the experimental displacement at failure. This may be as a result of the limited geometrically non-linear deformation occurring in the undamaged panel. Indeed, the linear elastic analysis was also shown to predict the strains accurately.

5.2 Damaged panel

It was seen for the damaged panel that the presence of the cut-out changes the load path significantly. Now, the load was seen to be carried mainly by the side stiffeners as well as by the skin around the cut-out. Furthermore, the stress and moment resultants were shown to be maximum around the cut-out. A peak in stress resultant was identified at the mid-length of the panel and at the edge of the cut-out and was in accordance with the experimental observation that the damaged panel failed by an in-plane compressive failure of the skin at this location. However, the calculated displacement at failure was shown to be about 28% lower than that measured experimentally.

The discrepancy between experimental and calculated results may be due to the coarse mesh used in the FE model. The stresses at the edge of a cut-out are strongly dependent on the mesh size and type. Another factor, other than the size of element, may be the type of elements used. Some triangular elements were used around the cut-out, as well as some distorted quadrilateral elements, and both may lead to poor results when used in a rapidly varying stress field, as around the cut-out. The use of higher order elements may help in these cases, although the distorted shape of the elements may cause inaccuracies in the calculations. Thus, a better agreement between calculated and experimental failure displacement may be achieved if the mesh around the cut-out were to be refined. It may also be noted that progressive damage of the region around the cut-out is expected to occur. The evolution of damage will effectively lead to a stress and strain redistribution, that could not be captured by the present analysis. A model including damage progression might well be necessary to predict accurately the correct displacement at failure.

5.3 Repaired panel

It was seen that the load path in the repaired panel had been restored using the present repair scheme. The repair has recovered the load-carrying capability of the central stiffener as well as that of the skin around the cut-out. A study of the contour plots did not reveal any peaks in value, nor did they suggest a potential position for failure initiation. Assuming that the repaired panel failed in the skin bays and in the repair patch, the calculated displacement at failure was 61% higher than in the experiment.

The poor agreement between the estimated and experimental failure displacement may be a result of the modelling approach used. The cut-out was ‘filled’ with two repair plugs (i.e. one for the skin and one for the stiffener) enveloped in adhesive to ensure that no clearance existed between the plug and the structure wall. The repair plug and its interaction with the wall of the panel was not taken into account in the present modelling approach, but it may be expected that the presence of the plugs will have an influence on the strength of the panels. Although the stress concentrations at the edges of the cut-out may be greatly reduced by the stress redistribution due to the repairs, a stress concentration at the edge of the damage will still exist. The clearance between the plug and the wall of the panel was 0.5mm but the interaction between the plug and the wall, when the panel is under load, will give rise to reduced stress concentrations around the cut-out. As a result, in-plane failure is still expected, but at a lower load than that calculated by the present FE model. It is noted that the interaction between the plugs and the wall of the panel cannot be modelled using the present idealisation. It may be considered that if failure results from the interaction between the plugs and the wall of the structure, the modelling approach used in the present work is not well adapted at estimating the failure load of the repaired panel.

6. CONCLUSIONS

The FE analysis method has been shown to be a good candidate to evaluate the behaviour of the panels. The quasi-3D shell element technique was employed to model one

undamaged, one damaged and one repaired panel. Two analyses were run for each model; one linear elastic and one geometrically non-linear elastic. For all types of panel studied, good correlations between the calculated and measured stiffness properties were observed for both analyses. However, the linear elastic analysis was inappropriate for evaluation of the strains in areas where significant out-of-plane deformation occurred. In such instances, the geometrically non-linear analysis led to the most accurate results.

The FE modeling revealed that the load path for the undamaged panel was such that load was carried by the skin as well as by the three stiffeners. Large out-of-plane deformations were seen to occur at the wide unsupported edges and in the skin bay of the undamaged panel. The presence of the cut-out changed the load path in the panels significantly, resulting in the load being carried mainly by the two side stiffeners and by the skin in the area adjacent to the damage. The present repair scheme was shown to restore the original load path in the panel, although it led to an over-stiffening of the skin bay. Potential failure locations were identified from the contour plots of the stress resultants and moment resultants.

For the undamaged panel, FE analyses showed that the stress and moment resultants were a maximum at buckle crests in the skin bays. These results from the FE analyses were combined with the Tsai-Hill criterion and successfully predicted the failure of the panel. For the damaged panel, the stress resultants were shown to be highest around the cut-out. With the present mesh, the failure displacement was calculated to be 28% lower than experiment. The disagreement was thought to be as a result of the coarse mesh used around the cut-out. In contrast to the two other panels, it was not possible to identify a potential failure site for the repaired panel. For the repaired panels the current FE models do not take into account the interaction of the repair plugs and the wall of the cut-out, where failure is thought to have initiated, and this leads to a poor prediction of the failure displacement from the combined FE/Tsai-Hill approach.

ACKNOWLEDGEMENTS

Funding by EPSRC is gratefully acknowledged. Many thanks go to BAe Airbus, BAe Systems, DERA, Hexcel, FEA Ltd., GKN WHL, GKN Aerospace and NPL for sponsoring this project and for supplying materials, structures and advice. The authors would like to thank Mr. H. MacGillivray for his assistance with the experimental studies. Sadly, Professor M. Crisfield died during the preparation of the present paper. His friendship and scientific contributions will be greatly missed.

SYMBOLS

E_i	Ply modulus in the i-direction
G_{ij}	Ply shear modulus in the i-j plane
ν_{ij}	Ply Poisson's ratio in the i-j plane

S_i	Ply tensile or compressive strength in the i -direction
S_{12}	Ply shear strength in the 1-2 plane
σ_i	Direct stress in the i -direction
σ_{12}	Shear stress

REFERENCES

- [1] S Mahdi, A J Kinloch, F L Matthews & M A Crisfield, "The Mechanical Performance of Repaired Stiffened Panels: Part 1 - Experimental Characterisation"
- [2] S Mahdi, "The Performance of Bonded Repairs to Composite Structures", PhD Thesis, Imperial College, London, February 2001.
- [3] S Mespoulet, "Through-Thickness Test Methods for Laminated Composite Materials", PhD Thesis, Imperial College, London, 1998.
- [4] M. Konig, "Mechanical Properties of 914C/T300" University of Stuttgart, Report BE-3444/BREU-0183.
- [5] H. Zhang, J. Motipalli, Y. C. Lam, and A. A. Baker, "Experimental and Finite Element Analyses on the Post-Buckling Behaviour of Repaired Composite Panels", *Composites Part A*, vol. 29A, pp. 1463-1471, 1998.
- [6] K. A. Stevens, R. Ricci, and G. A. O. Davies, "Buckling and Postbuckling of Composite Structures", *Composites*, vol. 26, pp. 189-199, 1995.
- [7] K. A. Stevens, S. Specht, and G. A. O. Davies, "Postbuckling Failure of Carbon/Epoxy Compression Panels", Proc 11th International Conference on Composite Materials (ICCM 11). Gold Coast, Australia, vol. 6/6, pp. 695-705, 1997.
- [8] K. A. Stevens, R. Ricci, and G. A. O. Davies, "Postbuckling Behaviour of Composite Compression Panels", Proc 19th ICAS Conference, ICAS-94-9.8.3. Anaheim, California, pp. 2975-2981, 1995.
- [9] B. G. Flazon, K. A. Stevens, and G. O. Davies, "Postbuckling Behaviour of a Blade-stiffened Composite Panel Loaded in Uniaxial Compression", *Composites Part A*, vol. 31A, pp. 459-468, 2000.
- [10] "LAP, Laminate Analysis Program", Anaglyph Ltd, Suite 33, 10 Barley Mow Passage, London W4 4PH, UK